ANL-7292

ANL-7292

Argonne National Laboratory

A METHOD FOR IDENTIFYING AND EVALUATING LINEAR DAMPING MODELS IN BEAM VIBRATIONS

by

M. W. Wambsganss, Jr., B. L. Boers,
and G. S. Rosenberg

DISCLAIMER

Printed in the United States of America
Available from
Clearinghouse for Federal Scientific and Technical Information
National Bureau of Standards, U. S. Department of Commerce
Springfield, Virginia 22151
Price: Printed Copy $3.00; Microfiche $0.65

ANL-7292
Physics (TID-4500)
AEC Research and
Development Report

ARGONNE NATIONAL LABORATORY
9700 South Cass Avenue
Argonne, Illinois 60439

A METHOD FOR IDENTIFYING AND EVALUATING LINEAR DAMPING MODELS IN BEAM VIBRATIONS

by

M. W. Wambsganss, Jr., B. L. Boers,
and G. S. Rosenberg

Reactor Engineering Division

April 1967

THIS PAGE
WAS INTENTIONALLY
LEFT BLANK

TABLE OF CONTENTS

LIST OF FIGURES

NOMENCLATURE

NOMENCLATURE

Symbol	Definition
c	Damping coefficient
f_D	Distributed damping-force intensity
ℓ	Length of beam
q	Generalized coordinate
r	Order of derivative corresponding to damping mechanism (see Eqs. 22, 23, and 24)
t	Time
x	Longitudinal displacement coordinate
y	Lateral displacement of beam, relative to the support
z	Lateral displacement of support
A	Cross-sectional area of beam
A_0	Amplitude of harmonic displacement of beam support
A_n	Amplitude of beam deflection at its nth resonant frequency
B_m	Mode-dependent constant (see Eq. 11)
E	Young's modulus for beam material
I	Moment of inertia of beam
R	Ratio of first- to second-mode magnification factors
Y	Absolute lateral displacement of beam
β	Ratio of forcing frequency to the modal natural frequency of the beam
γ	Modal phase angle (see Eq. 11)
ζ	Modal damping factor
θ	Modal phase angle (see Eq. 13)
λ	Eigenvalue (see Eq. 6)
μ	Modal magnification factor (see Eq. 21)
ρ	Mass density of beam material
ϕ	Eigenfunction (mode shape)
ω	Forcing frequency
ω_m, ω_n	Natural frequency of vibration for mth or nth mode

Subscripts	Refer to
1,2	First or second mode
k,m,n	Mode number
L	Load damping
S	Stress damping
V	Viscous damping
cr	Critical damping

Superscripts	Refer to
L	Load damping
S	Stress damping
V	Viscous damping

A METHOD FOR IDENTIFYING AND EVALUATING LINEAR DAMPING MODELS IN BEAM VIBRATIONS

by

M. W. Wambsganss, Jr., B. L. Boers,
and G. S. Rosenberg

ABSTRACT

This report presents the results of an effort to identify and evaluate effective linear damping models in beam vibration. The study was motivated by the desire to mathematically model the dynamic response of a beam-type element in which significant energy dissipation could be attributed to the contact of the component with adjacent similar components.

The usual method of modeling damping is employed, that is, assuming damping mechanisms and empirically evaluating the coefficients. The three damping mechanisms considered are designated viscous, stress, and load damping. The problem is that of identifying the dominant damping mechanism(s) for inclusion in the mathematical model, and of evaluating the associated damping coefficients.

A theoretical analysis is carried out, based on the usual assumptions in (Euler) beam theory and the further assumption of the damping being sufficiently small that the natural frequencies and mode shapes are unaffected. The analysis leads to a sensitive method, compatible with results obtained from tests on a vibration exciter, for identifying the effective damping mechanisms. The technique involves a comparison of the experimentally determined ratio of first- to second-mode magnification factors, related to a common point on the beam, with the constant values of this ratio corresponding to "pure forms" of the proposed damping.

The method is illustrated by application to the modeling of the response of a cluster of cantilevered beams clamped together at the base. This model is being employed in the preliminary analysis of the interaction effects of vibrating fuel rods in a nuclear-reactor core. Damping models are identified, and curves of damping coefficients as a function of cluster size are presented.

I. INTRODUCTION

A nuclear-reactor core is made up of many structural elements, usually in the form of slender plates or rods, which contain the fuel material. These fuel elements are often arranged in small subassemblies. These subassemblies, in turn, are mounted on a support grid, forming a relatively tightly spaced bundle. High-velocity coolant flows axially through this arrangement, and the entire core is additionally subjected to severe thermal and pressure loads.

Parallel coolant flow is known to induce oscillations of plates and rods. In a reactor, large amplitudes of oscillation must be avoided, not only for conventional structural reasons, but also because ensuing coolant-channel closure may have a critical effect on heat transfer and reactor neutron dynamics. In addition to flow-induced vibration, mobile reactors, to be used on submarines or space vehicles, are subjected to disturbances received from the environment in which the vehicle operates. This report stems from a part of the study directed toward acquiring pertinent design insights.

The mathematical modeling of the dynamic behavior of an in-core fuel assembly is complicated by the fact that interaction occurs among the clustered fuel subassemblies. Because of this interaction, and the fact that critical displacements are small, damping becomes an important consideration of the modeling.

The study of the interaction and damping using a full-size core mockup becomes prohibitive because of the high cost of fabricating prototype fuel assemblies. Therefore, as a preliminary model, the fuel subassemblies are simulated by hexagonal rods. The cluster is formed by clamping a rod bundle together at the base. Among the objectives of the study of this preliminary model are the following:

1. Determine the effect of cluster size on the natural frequencies and on damping of a rod within the cluster.

2. Identify damping models and associated damping coefficients to satisfactorily describe the dissipation of energy in a rod.

3. Determine the experiment size in terms of the number of elements in the experimental cluster that would be required to obtain experimental estimates of certain corresponding features (such as natural frequency and damping) without requiring the full prototype complement of cluster elements.

The damping force associated with the dissipation of energy can be a linear or nonlinear function of displacement, velocity, stress, temperature, and/or other factors. The mathematical modeling of this force is difficult, and the dynamicist must generally assume a damping mechanism and rely on empirical determination of the effective damping coefficients. The most widely used model, which leads to the simplest mathematical treatment, is

that of viscous damping, in which the damping force is assumed proportional to the velocity. Structural, or material, damping is often modeled assuming the damping force to be proportional to the displacement but in phase with the velocity. Various other damping mechanisms can be conceived.

This basic approach to modeling damping (that is, assuming damping mechanisms and utilizing empirical results for evaluation) is followed in studying the energy dissipated in the vibration of simulated fuel-assembly clusters. The three damping mechanisms considered are designated viscous, stress, and load damping. They are defined by the distributed damping-force intensity as

$$f_D(x,t) = \begin{cases} c_V y_t, \text{ viscous damping,} \\ c_S y_{xxt}, \text{ stress damping,} \\ c_L y_{xxxxt}, \text{ load damping,} \end{cases} \tag{1}$$

where the subscripts t and x refer to partial differentiation with respect to time and displacement, respectively. In the analysis, we assumed that the damping is sufficiently small that the natural frequencies and mode shapes are unaffected.

The selection of the dominant damping mechanisms is based on a comparison of the experimentally determined ratio of first- to second-mode magnification factors, with the constant values of this ratio corresponding to "pure forms" of the proposed damping, as obtained from theoretical considerations. The associated damping coefficients are evaluated by solution of a set of independent simultaneous equations. The set of equations is constructed by expressing the coefficients as a linear combination and using experimental results obtained at resonant conditions.

II. THEORETICAL ANALYSIS

A. Forced Vibration of a Lightly Damped Beam

Consider a transverse motion imparted to a uniform beam by giving the support the harmonic displacement,

$$z(t) = A_0 \cos \omega t. \tag{2}$$

With $y(x,t)$ defined to be the relative lateral displacement of the beam with respect to the support, the absolute displacement of the beam can be written

$$Y(x,t) = y(x,t) + z(t). \tag{3}$$

Including the three proposed damping mechanisms, and using Euler beam theory, the equation of motion for the beam becomes

$$EI \frac{\partial^4 Y}{\partial x^4} + C_L \frac{\partial^5 Y}{\partial x^4 \partial t} + C_S \frac{\partial^3 Y}{\partial x^2 \partial t} + C_V \frac{\partial Y}{\partial t} + \rho A \frac{\partial^2 Y}{\partial t^2} = 0 \qquad (4)$$

or

$$\frac{\partial^4 y}{\partial x^4} + \left(\frac{C_L}{EI}\right) \frac{\partial^5 y}{\partial x^4 \partial t} + \left(\frac{C_S}{EI}\right) \frac{\partial^3 y}{\partial x^2 \partial t} + \left(\frac{C_V}{EI}\right) \frac{\partial y}{\partial t} + \left(\frac{\rho A}{EI}\right) \frac{\partial^2 y}{\partial t^2} = -\left(\frac{C_V}{EI}\right) \frac{dz}{dt} - \left(\frac{\rho A}{EI}\right) \frac{d^2 z}{dt^2} \qquad (5)$$

For structural systems, the amount of damping is generally small. Based on this observation, the assumption will now be made that the relative motion of the beam can be represented as a superposition of the undamped free-vibration modes, or eigenfunctions, as found from solving

$$\frac{d^4 \phi_m}{dx^4} = \lambda_m \phi_m, \qquad \lambda_m = \frac{\rho A}{EI} \omega_m^2, \qquad (6)$$

with the appropriate boundary conditions. Therefore the relative motion of the beam can be written

$$y(x,t) = \sum_{k=1}^{n} \phi_k(x)\, q_k(t). \qquad (7)$$

Application of Galerkin's method by substituting Eq. 7 into Eq. 5, multiplying through by $\phi_m(x)$, and integrating over the length, gives, using the orthogonality property of the normal modes, a set of n ordinary differential equations to solve for the n generalized coordinates. In general, because of the nature of the stress damping term, the equations will be coupled. However, noting a further property[1] of the normal modes, that

$$\int_0^{\ell} \phi_m(x)\, \phi_n''(x)\, dx = 0, \qquad \text{for } (m+n) \text{ odd}, \qquad (8)$$

a two-term approximation to the motion, made up of an even and an odd harmonic term, will give uncoupled equations. Since a two-degree-of-freedom approximation often gives satisfactory results in slender beam vibrations, this requirement for uncoupling is not serious. Further, higher degree-of-freedom approximations may be used with this procedure when the stress-damping term is included, if it can be shown, say by an "order-of-magnitude" comparison, that the coefficients in front of the coupling terms are such that the coupling terms can be neglected relative to the remaining terms. With these comments regarding the uncoupling of the equations of motion, the analysis will be developed in general for an n-term, or n-degree-of-freedom, approximation, under the assumption that uncoupled equations can be obtained. The resulting set of uncoupled equations can be written

$$\ddot{q}_m + 2\zeta_m\omega_m\dot{q}_m + \omega_m^2 q_m = -(2\zeta_m^V\dot{z} + \ddot{z})\frac{1}{\ell}\int_0^\ell \phi_m(x)\,dx, \qquad (9)$$

where

$$\zeta_m = \zeta_m^V + \zeta_m^S\frac{1}{\ell}\int_0^\ell \phi_m\phi_m''dx + \zeta_m^L\frac{1}{\ell}\int_0^\ell \phi_m\left(\frac{d^4\phi_m}{dx^4}\right)dx$$

$$\zeta_m^V = \frac{c_V}{(c_{cr})_m}, \qquad \zeta_m^s = \frac{c_S}{(c_{cr})_m}, \qquad \zeta_m^L = \frac{c_L}{(c_{cr})_m},$$

$$(c_{cr})_m = 2\rho A\omega_m,$$

and the eigenfunctions have been normalized such that

$$\int_0^\ell \phi_m^2(x)\,dx = \ell. \qquad (10)$$

The steady-state forced vibration response to the sinusoidal forcing function (Eq. 2) can be written, using superposition, as

$$q_m(t) = B_m\left\{\cos(\omega t - \gamma_m) + \frac{2\zeta_m^V}{\beta_m}\sin(\omega t - \gamma_m)\right\}, \qquad (11)$$

where

$$B_m = \frac{A_0\beta_m^2\frac{1}{\ell}\int_0^\ell \phi_m(x)\,dx}{[(1-\beta_m^2)^2 + 4\zeta_m^2\beta_m^2]^{1/2}},$$

$$\gamma_m = \tan^{-1}\frac{2\zeta_m\beta_m}{1-\beta_m^2},$$

and

$$\beta_m = \frac{\omega}{\omega_m}.$$

The relative motion of the beam can then be represented by

$$y(x,t) = \sum_{m=1}^{n} B_m \phi_m(x) \left\{ \cos(\omega t - \gamma_m) + 2 \frac{\zeta_m V}{\beta_m} \sin(\omega t - \gamma_m) \right\} \quad (12)$$

or

$$y(x,t) = \sum_{m=1}^{n} y_m(x) \cos(\omega t - \gamma_m - \theta_m), \quad (13)$$

where

$$y_m(x) = A_0 \phi_m(x) \beta_m^2 \left\{ \frac{1 + 4\left(\frac{\zeta_m V}{\beta_m}\right)^2}{(1 - \beta_m^2)^2 + 4\zeta_m^2 \beta_m^2} \right\}^{1/2} \frac{1}{\ell} \int_0^{\ell} \phi_m(x)\, dx,$$

and

$$\phi_m = \tan^{-1} 2\left(\frac{\zeta_m V}{\beta_m}\right).$$

Therefore, the absolute motion of the beam is given by

$$Y(x,t) = A \cos \omega t + \sum_{m=1}^{n} y_m(x) \cos(\omega t - \gamma_m - \theta_m). \quad (14)$$

When vibration takes place at one of the natural frequencies, assume all the energy input goes into that mode of vibration. Under this assumption, when $\omega = \omega_n$,

$$Y(x,t) = A_0 \cos \omega_n t + y_n(x) \cos(\omega_n t - \gamma_n - \theta_n). \quad (15)$$

Also, when $\omega = \omega_n$, $\beta_n = 1$, which gives

$$y_n(x) = \frac{A_0 \phi_n(x)}{2\zeta_n} \left(1 + 4\zeta_n V^2\right)^{1/2} \frac{1}{\ell} \int_0^{\ell} \phi_n(x)\, dx, \qquad \gamma_n = \frac{\pi}{2} \quad (16)$$

and leads to

$$\frac{Y(x,t)}{A_0} = \cos \omega_n t + \frac{y_n(x)}{A_0} \sin(\omega_n t - \theta_n). \quad (17)$$

At a resonance, with small damping,

$$\left|\frac{Y(x,t)}{A_0}\right| \gg 1, \text{ and } 4\zeta_n^2 \ll 1; \tag{18}$$

therefore,

$$Y(x,t) \approx y_n(x) \sin \omega_n t, \tag{19}$$

where

$$y_n(x) = \frac{A_0 \phi_n(x)}{2\zeta_n} \frac{1}{\ell} \int_0^{\ell} \phi_n(x)\, dx.$$

When a beam is vibrated on a vibration exciter, the beam displacement at a resonance can be observed to be of the form

$$Y(x,t) = A_n(x) \sin \omega_n t, \tag{20}$$

where the amplitude $A_n(x)$ can easily be measured. Equating Eqs. 19 and 20 gives

$$\zeta_n = \frac{\phi_n(x) \int_0^{\ell} \phi_n(x)\, dx}{2\ell \mu_n(x)}, \tag{21}$$

where

$$\mu_n(x) = \frac{A_n(x)}{A_0}.$$

B. Damping-model Identification

Three damping mechanisms have been proposed in mathematically modeling the damping in a beam. The problem that now arises is that of identifying, from the three, the dominant damping mechanism(s). In this regard, it would be desirable to have a rather sensitive method of making the identification from simple experimental tests.

Assume, for the moment, that only one damping mechanism is dominant; take the other two damping coefficients to be zero. Then the remaining damping coefficient can be obtained from Eq. 21 as

$$c = \frac{\rho A \omega_n \phi_n(x) \int_0^{\ell} \phi_n(x)\, dx}{\mu_n(x) \int_0^{\ell} \phi_n \phi_n^{(r)}\, dx}, \tag{22}$$

where

$$c = \begin{cases} c_V, \text{ for } r = 0; \\ c_S, \text{ for } r = 2; \\ c_L, \text{ for } r = 4. \end{cases}$$

Equating the expressions for the damping coefficient (which is being assumed constant) as obtained from first- and second-mode considerations gives

$$R(x) = \left[\frac{\mu_1(x)}{\mu_2(x)}\right] = \left(\frac{\omega_1}{\omega_2}\right)\left[\frac{\phi_1(x)}{\phi_2(x)}\right]\left[\frac{\int_0^{\ell} \phi_1\, dx}{\int_0^{\ell} \phi_2\, dx}\right]\left[\frac{\int_0^{\ell} \phi_2 \phi_2^{(r)}\, dx}{\int_0^{\ell} \phi_1 \phi_1^{(r)}\, dx}\right]. \tag{23}$$

That is, the ratio of first- to second-mode magnification factors is a constant at a particular value of x, or section along the beam. When the eigenfunctions and the ratio of natural frequencies are known, the constant depends only on the order of the derivative of the eigenfunction under the integral, which in turn is directly related to the form of damping. Therefore, experimental determination of the ratio of magnification factors, related to a section on the beam, and comparison with the corresponding ratio constants, associated with a particular damping mechanism, gives a method of determining if one particular damping mechanism alone is present, or which two are dominant.

As an example, consider a clamped-free or cantilevered beam. The required modal properties* of beams are given in Ref. 2. Using these to evaluate Eq. 23 gives as the ratio of magnification factors, related to the tip of a cantilevered beam,

*An additional property, required in evaluating Eq. 23, is given in Ref. 1, that is,

$$\int_0^{\ell} \phi_m \phi_m''\, dx = \frac{1}{\ell}[\sigma_m \gamma_m \ell (2 - \sigma_m \gamma_m \ell)].$$

The symbols correspond to those in Ref. 2.

$$R(\ell) = \begin{cases} 0.288, \text{ viscous damping } (r = 0) \\ 4.46, \text{ stress damping } (r = 2) \\ 11.3, \text{ load damping } (r = 4) \end{cases} \tag{24}$$

Therefore, a comparison of the ratio of magnification factors gives a rather sensitive method, compatible with results derived from tests on a vibration exciter, for evaluating or selecting a damping model for a uniform beam.

Similar sets of ratio constants can be developed for beams mounted in various other basic configurations. Also, although it is not always practical, modes other than the first and second may be employed to give a ratio of magnification factors. The effect of shear and rotatory inertia, which has been neglected, increases with frequency. Therefore, if higher modes are used, care must be taken to be sure that the effective length (modal "wavelength") in comparison with the depth of the beam, is still such that slender-beam theory applies. Further, for the modal property given by Eq. 8 to hold, which allows stress damping to be included in general, an even and odd harmonic mode must be used.

In general, a two-mode approximation is often sufficient in the description of the dynamic response of most structural components. Unless the boundary conditions or type of excitation indicates that other modes might be expected, the two modes selected are generally the first and second. Therefore, it is logical to use the first- and second-mode magnification factors in the damping-model identification scheme.

C. Damping-coefficient Evaluation

Once the damping mechanisms and corresponding damping models have been selected, completing the formulation of the mathematical model requires evaluation of the associated damping coefficients. If a consideration of the ratio of magnification factors indicates, by a close comparison with one of the ratio constants given by Eq. 24, that only one form of damping is dominant, the corresponding damping coefficient can be readily evaluated with Eq. 22. In general, however, more than one type of damping will be indicated.

Equation 21 can be expanded and written in the form

$$c_V + c_S \frac{1}{\ell} \int_0^\ell \phi_n \phi_n'' \, dx + C_L \lambda_n^4 = \frac{\rho A \omega_n \phi_n(x) \int_0^\ell \phi_n(x) \, dx}{\ell \mu_n(x)}. \tag{25}$$

Let only two damping mechanisms be included in the model by assuming one of the damping coefficients to be zero. Vibrating a beam on a shaker through its first two resonant modes enables the corresponding natural frequencies and magnification factors to be measured. With this information and Eq. 25, two equations can be written and the two unknown damping coefficients can be computed.

As an example, consider once again the cantilevered beam, and let viscous and stress damping be the two damping mechanisms included in the mathematical model for the beam. With Eq. 25 and the properties previously given (in Ref. 2 and the footnote on p. 14) for a clamped-free beam, the viscous and stress damping coefficients can be expressed as

$$c_V = \frac{EI}{\ell^4}\left(\frac{18.2}{\omega_1 \mu_1(\ell)} - \frac{25.5}{\omega_2 \mu_2(\ell)}\right),$$

and

$$c_S = \frac{EI}{\ell^2}\left(\frac{1.37}{\omega_1 \mu_1(\ell)} + \frac{29.8}{\omega_2 \mu_2(\ell)}\right). \qquad (26)$$

In the above equations, the ratios of magnification factors are referred to the beam tip or free end. All that is required to compute the damping coefficients is a knowledge of the flexural rigidity and length of the beam and values for the first- and second-mode natural frequencies and magnification factors.

III. APPLICATION: REACTOR FUEL SUBASSEMBLIES

A. Experiment Design

As discussed earlier, the preliminary model, simulating the reactor fuel subassemblies, consists of a cantilevered cluster of hexagonal rods. The cantilevered configuration was chosen because, in a reactor, fuel subassemblies are frequently cantilevered from a support grid. A hexagonal cross section is typical of several reactor fuel subassemblies in addition to having a uniform section modulus about any axis and being readily available as a stock material. Therefore, a hexagonal cross section having 1/2 in. across the flats of the hexagon was used. The stock material purchased was selected so that a tolerance of ±0.001 in. on the 0.500-in. flat dimension was maintained.

Tests were conducted using both aluminum and steel rods. The effective length of the aluminum rods was $25\frac{3}{8}$ in.; the steel rods were 24 in. long. For this study, eight cluster sizes of 1, 7, 19, 37, 61, 91, 127, and 163 rods were tested. Figures 1 and 2 show the clamping fixture and a 37-rod cluster.

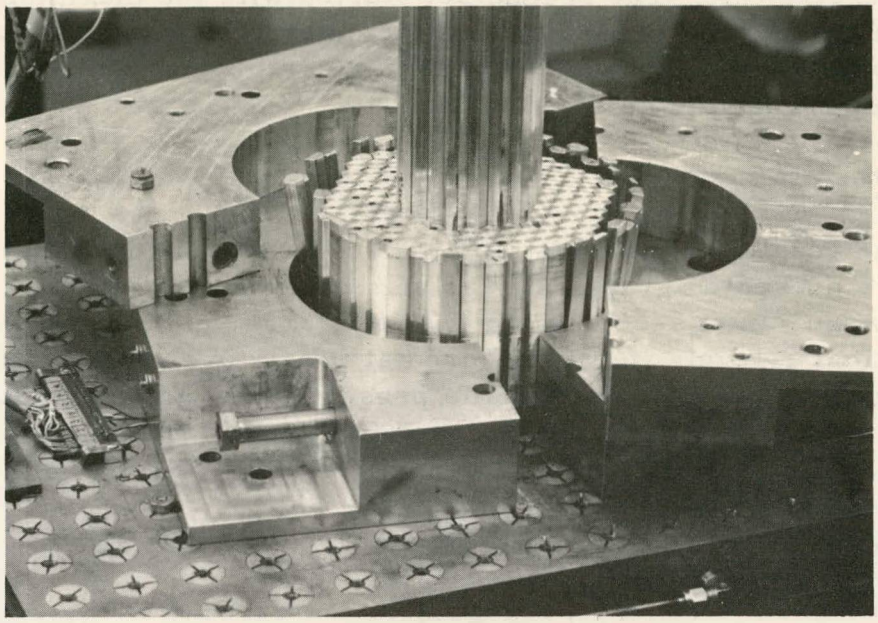

112-7179

Fig. 1. Clamping Fixture and Model Cluster

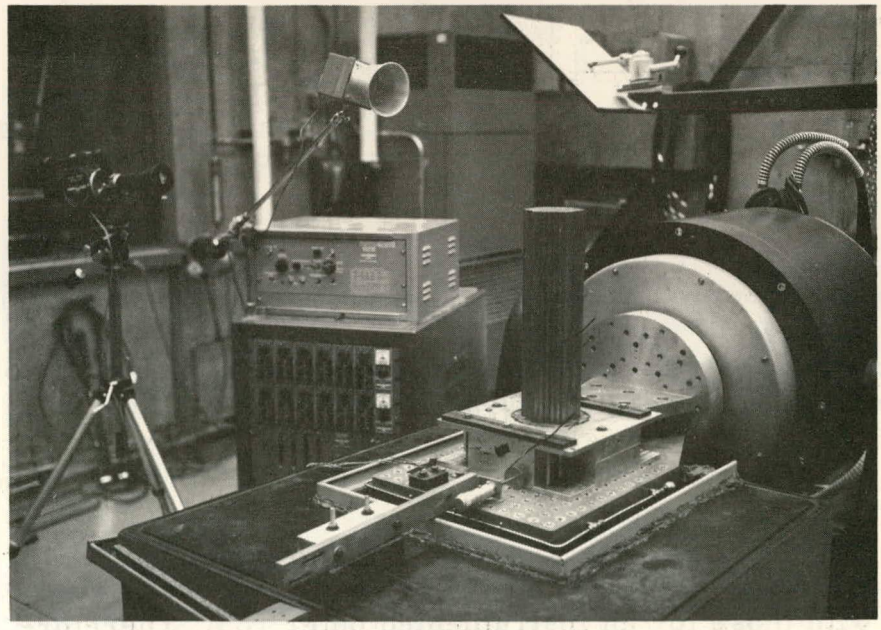

112-7180

Fig. 2. Experimental Test Setup

Three sets of tests were run with each type rod. In the first set, the initial cluster consisted of a single element and a row was added for each successive test. The second set started with the maximum-size cluster, and for each succeeding test the outer row would be removed and replaced with 4-in.-long stubs. In the third set of tests, the clusters were formed from randomly selected rods.

B. Test Results

The results of the tests, applicable to the subject matter of this report, are presented graphically as sets of curves in Figs. 3 and 4. When the tests were run at second mode with the larger clusters (61-163 rods), large vertical g-levels were measured at the fixture. The influence of these large vertical accelerations is present in the given results. The fixture or mounting must be redesigned for future tests.

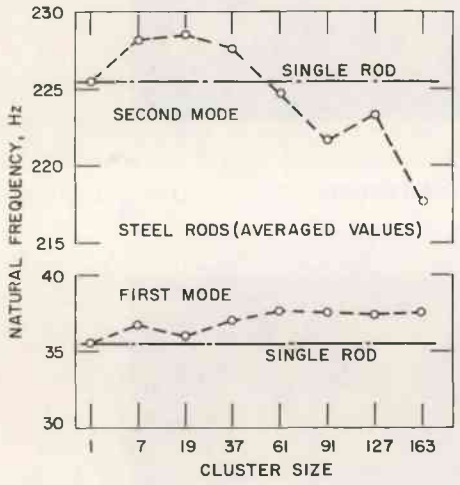

112-7141

Fig. 3. Natural Frequency vs Cluster Size

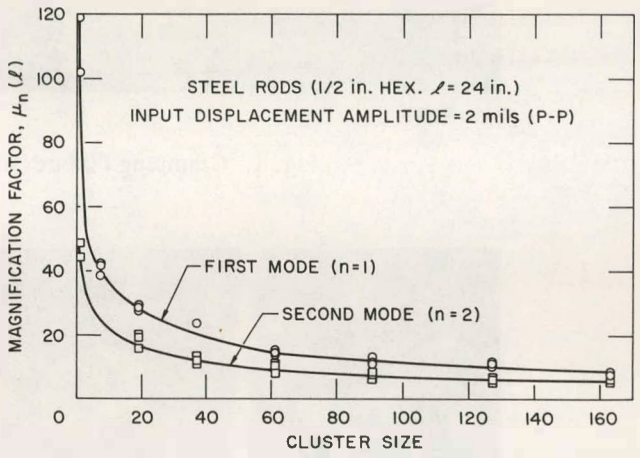

112-7144

Fig. 4. Magnification Factor vs Cluster Size

For this analysis, a natural frequency was assumed to be equal to the corresponding resonant frequency as defined by a maximum magnification factor. Figure 3 shows that the natural frequencies of vibration of a rod in a cluster do not vary significantly from the corresponding natural frequency of a single rod.

The strain-versus-frequency plots for the center rod compared favorably with those for an instrumented outer rod. Therefore, it was assumed that an outer rod was representative of the behavior of a typical rod in a given cluster. This was an advantage in data reduction. The outside rod could easily be instrumented with a miniature accelerometer, and since acceleration is proportional to displacement, for the harmonic response at resonance, the magnification factor becomes simply the ratio of tip-to-input acceleration. Figure 4 is a plot of the first- and second-mode magnification factors calculated in this manner.

As illustrated in Fig. 4, as the number of rods in the cluster is increased from one to the maximum of 163, the magnification factors decrease continually. Sensitivity of the magnification factor to input amplitude is ruled out by the fact that a controlled constant-amplitude input was used. Therefore, the difference in response between a single rod and a rod in a multirod cluster is dominated by the increased dissipation of energy with increasing cluster size; hence, damping must be included in the equation of motion for a fuel assembly.

The theoretical analysis, developed in Section II-A of this report is based on the assumption that the natural frequencies and mode shapes are unaffected by the damping. Figure 3 shows that the natural frequencies remained relatively constant with cluster size. Based on this observation, we would intuitively expect the mode shapes to also remain effectively unchanged.

C. Rod Mode-shape Tests

Since the analysis assumes that all rods in a cluster move as a single cantilever, it was desirable to verify this fact experimentally.

Strain gages mounted in milled-out portions of the rod were used to give bending strain at the quarter points of the rod. The rod was excited alone and as the center rod in a cluster of 19 and a cluster of 91 rods. The theoretical strain values were calculated using Ref. 2. Figure 5 is a plot of the results. Note that the strain values departed from the theoretical somewhat when the rod was excited as a member of a cluster. We did not calculate the effect of this variation in ideal motion on the damping action of the rods.

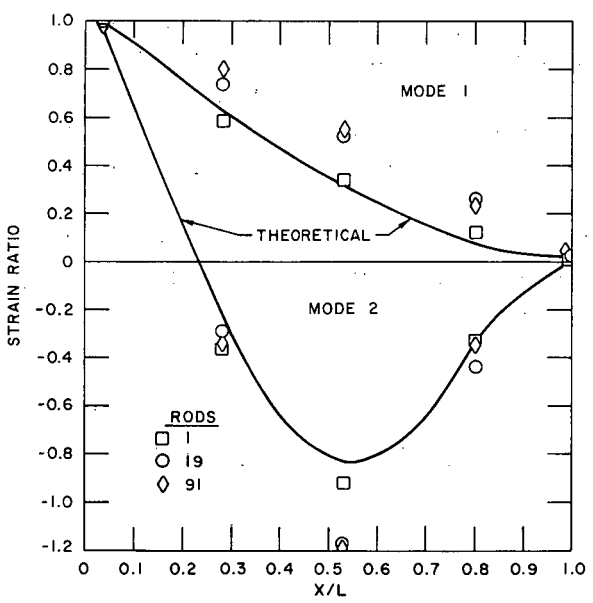

Fig. 5. Mode-shape Comparison

Strobe lights and a pulse camera were used to photograph the rod-cluster motion at resonance. Slow-motion projection of this film provides quantitative evidence that the cluster's overall motion is the same as that of a single rod. The individual rods in a cluster also move as a single rod, often out of phase with other rods in the cluster. This results in severe rod clatter at resonance and significant damage to the rods. This rod damage could become severe in a mobile reactor. The out-of-phase motion and consequent rod interaction undoubtedly account for much of the deviation of the experimental strain levels from those calculated or those of a single rod.

D. Damping-model Identification

To model the damping, the three damping mechanisms given by Eq. 1 were considered. The method developed earlier, for identifying linear damping models using test results obtained on a vibration exciter, will now be applied to determine the dominant damping mechanisms, describing the dissipation of energy that occurs during the vibration of simulated fuel subassemblies.

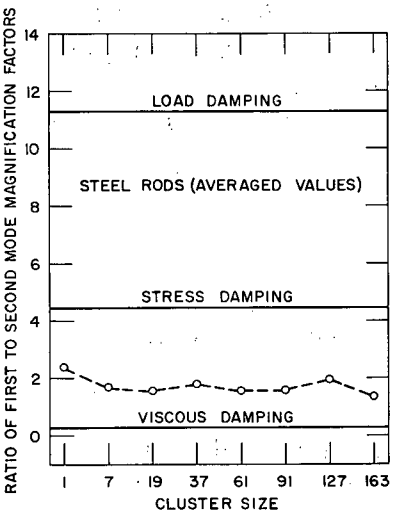

112-7143

Fig. 6. Ratio of First- to Second-mode Magnification Factors as a Function of Cluster Size

The identification scheme is based on the comparison of the ratio of first- to second-mode magnification factors with theoretically determined constants corresponding to "pure" forms of the proposed damping mechanisms. Using the averaged experimental data points given in Fig. 4, we can calculate the ratios of first- to second-mode magnification factors. The results are given in Fig. 6, where comparison can be made with ratio constants corresponding to pure viscous, stress, and load damping as obtained from Eq. 24.

The experimental data lie between the lines corresponding to viscous and stress damping. Therefore, it is deduced that these may be the two dominant damping mechanisms to be included in the equation of motion for a fuel subassembly. The ratio of first- to second-mode magnification factors is employed as a means of identifying the damping mechanisms present. Since the experimentally determined ratios are approximately constant, and hence independent of cluster size, we may conclude that the damping mechanisms themselves are invariant with cluster size.

In summary, based on a consideration of the ratio of magnification factors, viscous and stress damping are assumed to represent the dominant energy-dissipative mechanisms.

E. Damping-coefficient Evaluation

The damping models (that is, viscous and stress damping) having been selected, the remaining problem is to determine the appropriate damping coefficients to use in the models. This is easily accomplished by substituting the experimental results into Eq. 26, which was derived for a cantilevered beam. The magnification factors averaged over the three sets of tests were used. The damping coefficients, so calculated, are plotted against cluster size in Fig. 7.

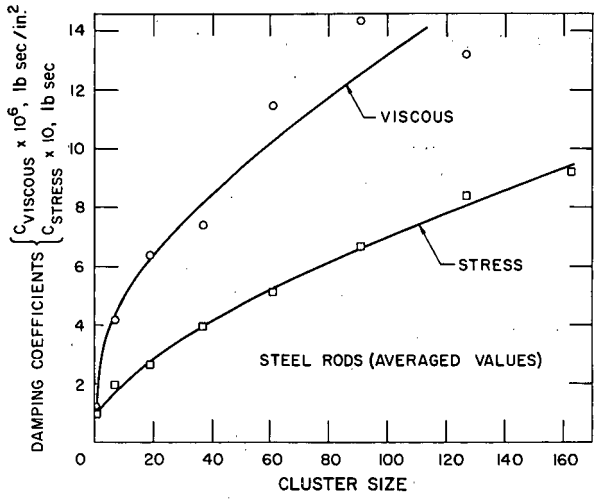

112-7142

Fig. 7. Damping Coefficient vs Cluster Size

With the results given in Fig. 7, a two-mode, or two-term, approximation for the equation of motion of a rod in a particular-size cluster can be written including damping. The response to an arbitrary input, say, p(x,t), which might result from a pressure loading, would take the form

$$y(x,t) = \phi_1(x)\, q_1(t) + \phi_2(x)\, q_2(t). \tag{27}$$

The generalized coordinates are determined by solving

$$\ddot{q}_m + 2\zeta_m \dot{q}_m + \omega_m^2 q_m = \frac{\int_0^{\ell} p(x,t)\, \phi(x)\, dx}{EI\ell}, \tag{28}$$

where

$$\zeta_m = \frac{1}{2\rho A \omega_m}\left\{c_V + c_S \frac{1}{\ell}\int_0^{\ell} \phi_m \phi_m''\, dx\right\},$$

and the coefficients c_V and c_S are read from Fig. 7 for the particular-size cluster.

F. Model Size of a Reactor Core

The objective of this experiment was to develop a method for analysis of response of a reactor core (fuel element and support structure) to vibration or shock loading. A preliminary step in such an analysis is to determine experimentally how complicated a model of the system must be to provide order-of-magnitude response data to a designer. That is, can a simple model provide an early indication of the response of a proposed system? In a reactor core, complexity is increased by, among other factors, the number of fuel elements used. Also, a major portion of the cost of core test specimens is the fuel elements. Thus if a model can predict the order-of-magnitude response and how much of the core need be tested to obtain exact data, a considerable economy in cost and reduced complexity is achieved.

This experiment can be used to attempt to answer the question: How many actual fuel elements must a test specimen contain in order to predict response of the entire core? Response of the core in this report

was determined by magnification factor (output over input) of the simulated fuel elements. Figure 6 shows the ratio of first- to second-mode magnification factors to be almost constant. Since the ratio of magnification factors is essentially a constant for more than one element, testing for second-mode response need only be done once with actual reactor fuel elements. This is an advantage, since for a constant-input displacement the acceleration level goes up as a function of the frequency squared. Since the ratio of second natural frequency to first can be expected to be 6.27 for a cantilever, the acceleration level or force will increase 39.3 times that at first-mode resonance. Thus the possibility of damage to the fuel elements is much reduced by elimination of testing at second-mode resonance.

A plot of magnification factor versus cluster size (Fig. 4) shows that the change in magnification factor is reduced with increasing cluster size. This indicates that one need not test the entire core of a reactor; however, the amount of testing at present does not allow selection of a cluster size above which one need not test.

IV. SUMMARY AND DISCUSSION

A study of the dynamic response of reactor fuel-assembly clusters, indicated the importance of including damping in the model. The effort to model the damping led to the development of a method for identifying assumed damping mechanisms and calculating the associated damping coefficients. The method is based on a comparison of experimental results with theoretically determined values. The required experimental results are easily obtained from tests performed on a vibration exciter. The method is sensitive to the ratio of first- to second-mode magnification factors and appears well-suited to formulating mathematical models for structural components, amenable to vibration testing, which can be modeled as two-degree-of-freedom systems.

Experimental results were obtained using a constant displacement-amplitude input. Linearity is assumed in the mathematical model and in application should be checked experimentally by investigating the dependence of the magnification factor on the displacement amplitude of the input. Also, when such tests are conducted, fixture or connection damping is included implicitly in the results. In certain cases, this may be desirable. However, to be able to obtain quantitative results from such tests, the test must bear close resemblance to the final application.

The mathematical model, formulated in the manner outlined in this report, has been forced to give the correct response at the first two natural frequencies for the given input. This results from using information obtained while operating at the resonances to compute the required damping

coefficients. Since a system is most sensitive to damping at, or near, a resonant frequency, it may be reasonable to expect the mathematical model to satisfactorily predict the dynamic response throughout the frequency range for which the model is derived. The ability of the mathematical model to predict system response to arbitrary loadings must be checked by experiment.

Any two damping models might have been chosen and the coefficients forced to give the required responses at the resonances. However, the proposed models of viscous, stress, and load damping do have certain physical significance. Also, the location of experimental data in relation to the theoretical values on the plot of the ratio of magnification factors versus cluster size, lends support for the use of these models to represent the energy-dissipative mechanisms.

With regard to satisfying the objectives of the study, the following concluding remarks can be made:

1. The cluster size, and hence, the interaction phenomena, has little, if any, effect on the natural frequencies of an individual element within the cluster.

2. The magnification factor, related to the free end of the rod, decreases continuously with cluster size, but appears to be approaching a limiting value.

3. In the attempt to determine the experiment size required to give results typical of a full-size core, the only invariant observed was the ratio of first- to second-mode magnification factors. This is the ratio that is employed in the damping-model identification scheme. The magnitude of this ratio indicates that viscous and stress damping may be the dominant damping mechanisms.

APPENDIX

Experimental Studies

A. Fixture Design

As with all vibration testing, the fixture design was an important consideration for good results and ease of data acquisition. Making a truly fixed end for a cantilever is difficult. To determine feasibility of this type experiment, we decided to make a fixture that would clamp the lower 4 in. of the rods and be adaptable to one cantilever or the full eight rows of them. To reduce balancing problems, we used a slip-plate type setup.

The clamping fixture consisted of two square 2-in.-thick plates of aluminum, which had an 8-in. hole in the center. The plates were cut into two parts and bolted together and to the slip plate of the shaker. The cluster of hexagonal rods was made one row larger with 4-in.-long stubs and then turned down to an 8-in. diameter. Thus the fixture could clamp on the lower 4 in. of the rods. The fixture could be used for any number of rows by replacing rods with 4-in. stubs as desired. The centerline of the shaker's armature was attached to the top of the fixture, and the slip plate was attached at a lower point on the armature. This reduced the inertial rotational moment, tending to lift the free end of the slip plate, since the force input was approximately 5 in. higher than it would have been by inputting the force at the slip plate. This system exhibited fixture resonance with no rods of about 290 Hz.

B. Clamping Force

Figure 1 shows the method of clamping. The clamping was the same from test to test, regardless of the number of rows of rods being tested.

To determine the required torque level on the clamping bolts which would provide adequate axial restraint to a rod in a cluster of rods, a clamping test was performed. The fixture was mounted so that a static load of known magnitude could be exerted upon the center rod of a cluster. The clamping bolts have an internally mounted strain-gage bridge, which provided a relationship between tightening torque and axial bolt elongation. This measurement is difficult because of the variation in friction of mating threads. Molybdenum disulfide was used as a lubricant to reduce this problem. All bolts were tightened to a uniform strain level, and the values of torque required were recorded. The static load on the rod to initiate motion (overcome static friction) was plotted against the average torque applied to the bolts. The data can be represented by the relationship

$$\text{Torque (in.-lb)} = 0.643 \text{ force (lb)} - 14.3.$$

Since for the damping-determination experiments it was time-consuming to measure bolt elongation, 1200 in.-lb of torque was used for all experiments. According to the above relation, this provides 1890 lb of axial restraining force on each rod.

C. Test Procedure

The desired number of rods were mounted in the fixture, and a torque wrench used to tighten the fixture to the previously discussed level. The shaker servo control was then used to maintain a constant input displacement during the preprogrammed frequency sweep. Data acquisition and reduction are discussed in the following paragraphs.

1. Servo Displacement-control System

Figure 8 is a block diagram of the basic control system used to maintain constant displacement during the rod tests. The circuits isolated by the dashed lines are part of the Honeywell data-reduction complex. The diagram has been simplified in that only the primary circuits are shown.

The displacement signal originates in a Photocon displacement transducer (a capacitance device), mounted adjacent to the clamping fixture and using the fixture as one plate of a capacitor. The voltage output (analogous to displacement) from the transducer is transferred to the spectrum analyzer by ~300 ft of coaxial cable. The spectrum analyzer contains a tracking filter with an adjustable bandwidth. This filter performs several stages of modulation and demodulation on the input voltage, and outputs a high-frequency signal with an amplitude corresponding to the amplitude of the fundamental input voltage. Thus the output amplitude is not affected by the noise and harmonic distortion of the input signal. The detector module provides a dc voltage for the X-Y plotter and feeds the automatic amplitude control. This module's sinusoidal output is adjusted in magnitude and returned to the shaker as a control signal. The sweep oscillator module controls the frequency of this output. Thus the system can sweep over a preset frequency band at a predetermined rate maintaining a constant displacement amplitude of motion output of the shaker.

The displacement transducer is calibrated by setting an acceleration level at an appropriate frequency, thus providing the desired displacement motion. The acceleration signal originates in an Endevco crystal-type accelerometer and is amplified by a charge amplifier, which drives the long lines to the Honeywell equipment. In these tests, a peak acceleration level of 2 g's at a frequency of 140 Hz was used, and the resultant displacement transducer signal adjusted to provide a peak-to-peak displacement of 2×10^{-3} in., which can be calculated from

$$\text{Acceleration} = 0.0511\ (\text{freq})^2\ \text{disp.}$$

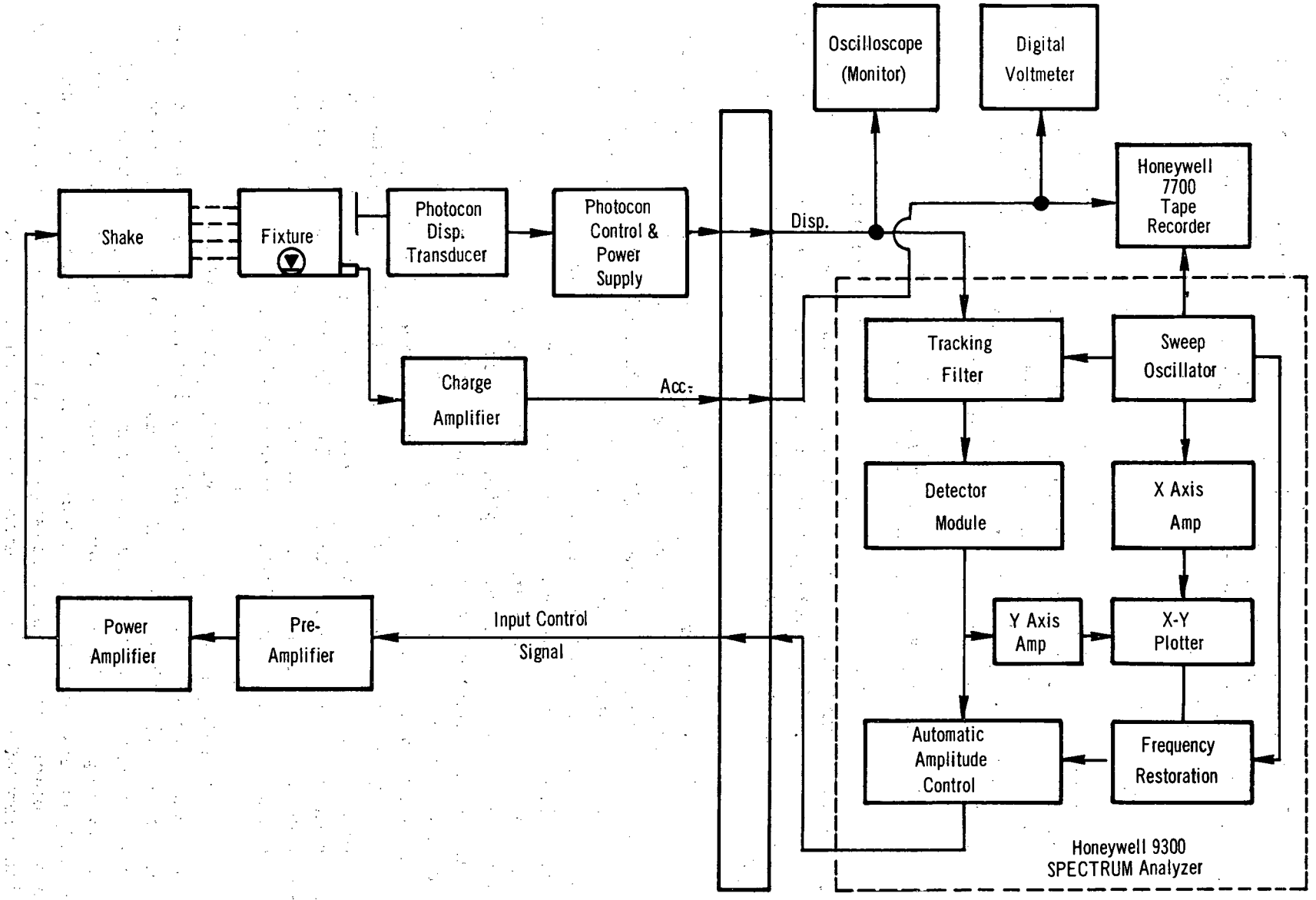

Fig. 8. Block Diagram of Servo System

At various times throughout the experiment, the servo-system accuracy was checked. Acceleration input to the test specimen was plotted and compared to that predicted by the previous equation. Normal deviation was less than ±3% from the calculated values. The exception to this accuracy was at frequencies corresponding to the second natural frequency of the rods being tested. The resonating rods exerted inertial torques on the fixture and caused significant vertical motion. Thus the displacement transducer added a component of this motion to the horizontal motion. The deviation caused by this phenomenon is estimated to be less than 10% reduction of horizontal motion.

2. Data Acquisition

Three methods of data acquisition were used. Accelerometers provided input acceleration level on the fixture, and rod acceleration at the top of the cluster. Strain gages were mounted on the rods of interest. Displacement of the fixture was monitored by the Photocon displacement transducer, which operates on the changing-capacitance effect between the fixture and the transducer. The Photocon device can resolve 1×10^{-4}-in. displacements. Figure 9 is a block diagram of the strain and acceleration data-acquisition system.

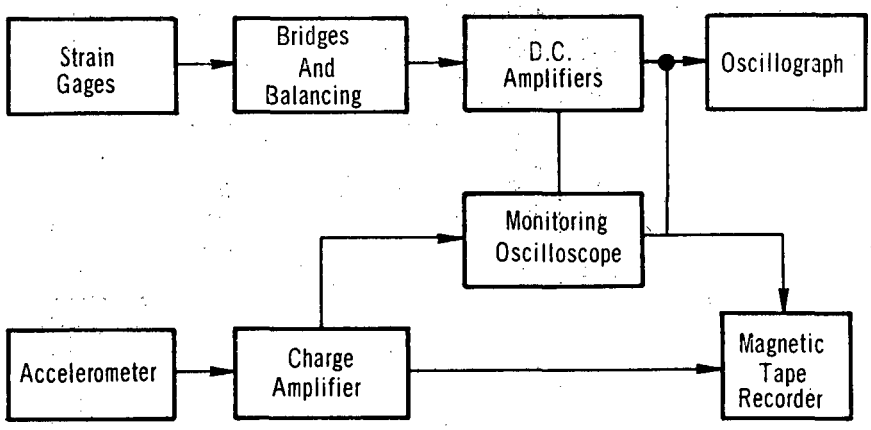

Fig. 9. Block Diagram of Data-acquisition System

The accelerometers were Endevco piezoelectric crystal type. Three Model 12217 accelerometers for fixture monitoring in all three axis and a Model 2222 accelerometer for rod-top acceleration were used. Endevco charge amplifiers (Model No. 2713A) provided signal levels appropriate for the Honeywell 7700 tape recorder. All accelerometers were comparison-calibrated to a factory-calibrated accelerometer before the experiment started.

Foil-type strain gages, manufactured by Baldwin-Lima-Hamilton, Inc., were applied with Eastman 910 adhesive. The bridges and balancing circuits were built at ANL. Dana Model 2200 dc amplifiers provided signal levels appropriate for the Honeywell tape recorder and/or a 36-channel Consolidated Electronics Corporation oscillograph. Magnitudes of the final record compared to within 5% for the two recording devices. The strain gages were calibrated by the parallel-resistance method for changing gage resistance. Calibration points used were 0, 500, and 2000 μin./in. of simulated change.

3. Data Reduction and Presentation

The information provided during each test was as listed:

Displacement	Fixture base (servo-controlled)
Acceleration	Fixture base (three axes) Rod top
Bending Strain	One center rod One outer rod

Figure 10 is a block diagram of the data-reduction system. The data were recorded on tape at 3.75 in./sec. At this speed, the frequency response of the tape recorder is dc to 2500 Hz.

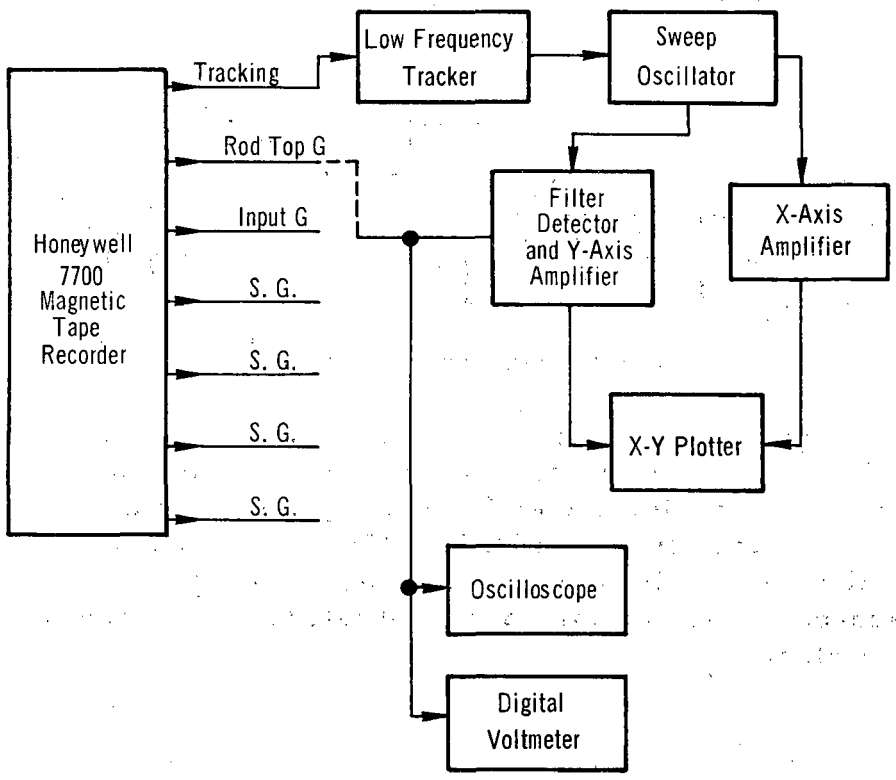

Fig. 10. Block Diagram of Data-reduction System

The reproduced data were filtered before analysis using a 50-Hz bandwidth with a detector time constant of 0.1 sec. The wide bandwidth and small time constant prevented the loss of data during the rapid changes caused by specimen resonance. Frequency sweep time was 9.6 sec/Hz during resonances, and from 0.28 to 1.06 sec/Hz during other portions of the frequency span.

Curves of rod-top (output) acceleration divided by fixture (horizontal input) acceleration were plotted on a logarithmic scale against frequency on a linear scale. Preadjustment of the charge amplifiers provided the required scale factors.

The four strain-gage signals were also plotted from the tape as a function of frequency. Calibration signals were recorded on the tape before the test. Those signals were generated using the resistance calibration method previously discussed. Figures 11, 12, and 13 are examples of the data plotted.

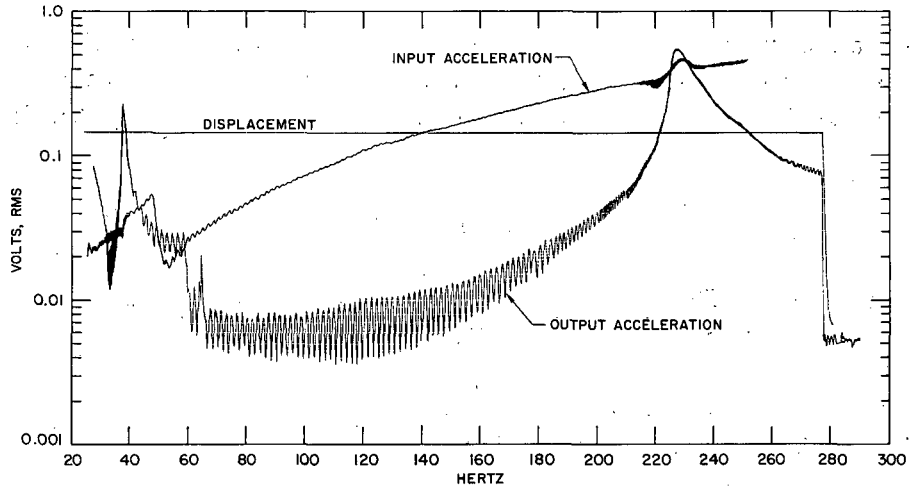

Fig. 11. Plots of Acceleration and Displacement

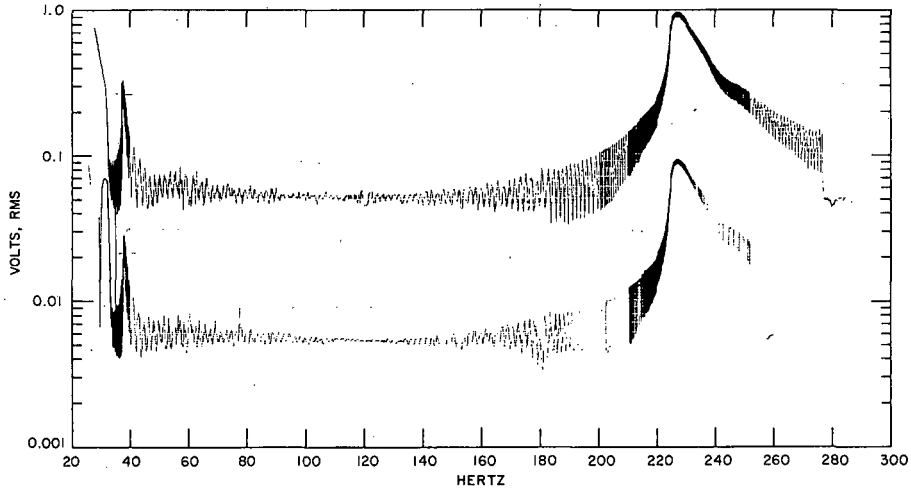

Fig. 12. Bending Strain of Center Rod

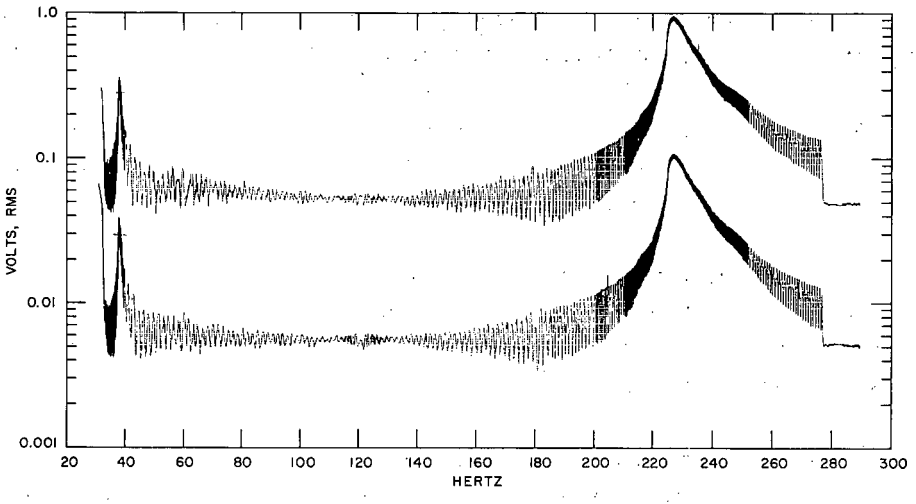

Fig. 13. Bending Strain of Outer Rod

ACKNOWLEDGMENTS

The authors acknowledge Messrs. J. A. Jendrzejczyk, W. Lawrence, and K. E. Stair for performing the experiments on the vibration exciter, solving various instrumentation problems, and processing the data.

REFERENCES

1. H. L. Langhaar, Energy Methods in Applied Mechanics, John Wiley and Sons, New York (1962), p. 283.

2. R. E. D. Bishop and D. C. Johnson, Vibration Analysis Tables, Cambridge University Press (1956).